



PCCP

**Spectroscopic studies of kinetically trapped conformations
in the gas phase: the case of triply protonated bradykinin**

Journal:	<i>Physical Chemistry Chemical Physics</i>
Manuscript ID:	CP-ART-03-2015-001651.R1
Article Type:	Paper
Date Submitted by the Author:	24-Apr-2015
Complete List of Authors:	Voronina, Liudmila; École Polytechnique Fédérale de Lausanne, Laboratoire de Chimie Physique Moléculaire Rizzo, Thomas; École Polytechnique Fédérale de Lausanne, Laboratoire de Chimie Physique Moléculaire

SCHOLARONE™
Manuscripts

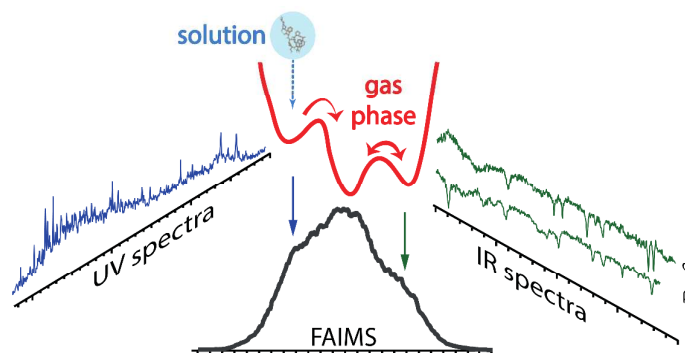
Spectroscopic studies of kinetically trapped conformations in the gas phase: the case of triply protonated bradykinin

Liudmilla Voronina and Thomas R. Rizzo

*Laboratoire de Chimie Physique Moléculaire, École Polytechnique Fédérale de Lausanne, EPFL SB
ISIC LCPM, Station 6, CH-1015 Lausanne, Switzerland*

Abstract

Understanding the relation between the gas-phase structure of biological molecules and their solution-phase structure is important when attempting to use gas-phase techniques to address biologically relevant questions. Directly after electrospray ionization, molecules can be kinetically trapped in a state that retains some “memory” of its conformation in solution and is separated from the lowest-energy gas-phase structure by barriers on the potential energy surface. In order to identify and characterize kinetically trapped structures, we have explored the conformational space of triply protonated bradykinin in the gas phase by combining field-asymmetric ion mobility spectrometry (FAIMS) with cold ion spectroscopy. We isolate three distinct conformational families and characterize them by recording their UV-photofragment spectra and vibrational spectra. Annealing of the initial conformational distribution produced by electrospray reveals that one of the conformational families is kinetically trapped, while two others are stable, gas-phase structures. We compare our results to previously published results obtained using drift-tube ion mobility spectrometry (IMS) and propose a correspondence between the conformational families separated by FAIMS and those by IMS.



1 Introduction

Mass spectrometry (MS), ion mobility spectrometry (IMS), and laser spectroscopy are all widely used to study biological molecules in the gas phase.¹⁻⁸ In contrast to many solution-phase techniques, these gas-phase methods can be implemented in such a way that they don't average over an ensemble of conformations, but allow investigation of each of the structures separately. This could be especially valuable for systems that lack well-defined structure, such as intrinsically disordered proteins or peptide oligomers,⁹⁻¹¹ which tend to have several different conformations in solution with differing biological activity. Such molecules can adapt to their local environment and change their structure to perform a particular function.¹²

Although gas-phase techniques are widely used to address biological questions, there is debate about the relation between the gas-phase structure of biological molecules and their solution-phase structure.¹³⁻²² While Jarrold suggested in the 90's that mass-spectrometry "may provide a quick and sensitive tool for probing the solution phase conformations of biological molecules",²³ the range of validity of this statement is still under discussion. There are several types of evidence that some features of solution-phase conformation of a peptide or protein can be preserved when molecules are transferred to the gas phase *via* electrospray. For one, collisional cross-sections (CCS) of ions sprayed from native conditions are often close to those calculated for the crystal structure.²⁴⁻²⁶ Moreover, ions produced from denaturing and native conditions exhibit different properties, such as their charge state distribution, CCS, the degree of gas-phase H/D exchange, or their fragmentation patterns.^{21, 27-30} Finally, gas-phase biomolecular ions have been shown to undergo structural changes (i.e., unfolding and re-folding) while trapped in a mass-spectrometer^{31, 32} or upon collisional activation.³³⁻³⁵ This means that one can produce and preserve metastable species that are significantly different from the lowest energy gas-phase structures and are kinetically trapped, with barriers on the potential energy surface that inhibit them from isomerizing. Using a cryogenic ion-mobility spectrometer, Silveira et al. have recently provided evidence of kinetic trapping of triply protonated substance P in the gas-phase on the time scale of milliseconds after dehydration.^{22, 36, 37} All these experiments imply that the molecules retain some "memory" of their state in solution and/or that during the ESI process.¹³ Determining whether solution-phase structures can be trapped and studied in the gas phase is important for evaluating the relevance of powerful, conformer-specific gas-phase techniques for biological applications. If significant structural elements can be preserved in the gas phase, one could

2 Experimental approach

We first generate gas-phase ions by electrospray, separate them into conformational families by FAIMS,^{51, 52} and then inject them into our cold-ion spectrometer where we perform spectroscopic studies at cryogenic temperatures.⁴¹ Separation of ions in FAIMS is based on the difference in their mobility at high and low electric fields. A detailed description of the separation process can be found elsewhere.^{51, 53} Briefly, ions are dragged by a carrier gas between two electrodes. An asymmetric waveform consisting of alternating periods of low and high voltage of opposite polarity is applied across these electrodes such that the time-averaged potential difference between them is zero. Because the mobility of ions in high and low electric fields is typically different, the ions drift in a direction perpendicular to the electrodes. To offset this drift a small compensation voltage (CV) is applied between the electrodes, and scanning this voltage produces a CV “spectrum”, as conformers of the same ion can have different ion transport properties. In this study we use FAIMS of the “side-to-side” geometry (Thermo Scientific), which has higher transmission efficiency compared to flat-electrode FAIMS because of atmospheric ion focusing.⁵⁴ Nitrogen is used as the carrier gas with a typical flow rate of 2 l/min, and the waveform amplitude (dispersion voltage) is set to 5000V. The temperature of the electrodes is kept at 25°C.

Ions transmitted through the FAIMS stage are injected into a home-built cold-ion spectrometer.⁴² After passing through a metal capillary, they are focused by an ion funnel⁵⁵ operated at a pressure of 1.5 mbar. When necessary, we can also use the funnel for in-source ion activation by increasing the RF amplitude. Excitation mainly occurs at the end of the funnel where the diameter of the electrodes is smallest.⁵⁶

After being extracted from the funnel, the ions are pre-stored in a room-temperature hexapole ion trap for 70 ms, mass-selected by a quadrupole mass-filter, and then guided into a cold (4 K) octopole ion trap, where they are cooled by collisions with helium. A UV laser pulse promotes the trapped ions to the first electronically excited state, and since the excitation energy is above the dissociation threshold, some of the parent ions fragment. All the ions are then ejected from the trap, mass-selected by a second quadrupole filter, and detected by a channeltron. Detecting the number of ions in a specific fragmentation channel as a function of wavelength gives an electronic photofragment spectrum of the parent molecule. As BK has a low photofragmentation yield, we add a CO₂ laser pulse after UV excitation to enhance it.⁵⁷ The electronic spectrum is then recorded as the difference between the fragment signals produced by the UV laser pulse combined with the CO₂ pulse

and those from CO₂ laser alone. The most abundant UV laser-induced fragment results from the loss of the phenylalanine side chain (i.e., via C_α – C_β bond breakage), and we use this fragmentation channel for all measurements.

To obtain conformer-selective IR spectra of the ions, we set the UV laser on a specific transition in the electronic spectrum and introduce an IR pulse from a tunable OPO 200 ns before the UV pulse. This results in depletion of the photofragment signal that is recorded as a function of IR wavelength.⁴⁴

Bradykinin (RPPGFSPFR, acetate salt, 98%, Sigma Aldrich) was purchased and used without further purification. Peptide solutions were prepared in a 49:49:2 mixture of water:methanol:acetic acid with a bradykinin concentration of 50 μM. In the 3+ protonation state, the extra protons are believed to reside on the two arginine side chains and on the N-terminus.⁵⁸

3 Results and discussion

Ion mobility studies of triply protonated bradykinin (BK³⁺) by Clemmer and coworkers reveal three primary conformational families in the gas-phase, which they call A, B and C, and several elongated structures that each represent less than 5% of the population.³³ Under normal conditions, the population distribution among the three main families was found to be 22:31:31 respectively. Under conditions in which they anneal the conformer populations by collisional activation to a “quasi-equilibrium” (QE) distribution, this ratio changes to 1.8:16:80. They obtain the same ratio if they first isolate a single conformation and then subject it to the annealing process. In a separate publication they have also shown that the conformer distribution initially produced in the gas phase depends upon the solvent from which they are sprayed.¹⁹

3.1 FAIMS separation of BK³⁺

In this study we have separated the conformational families of BK³⁺ by means of FAIMS. Figure 1(a) represents the CV distribution recorded by detecting all transmitted ions as a function of the compensation voltage. The line shape of this spectrum clearly suggests the presence of at least three distinct conformational families. While the features are not fully resolved, one can use photofragment spectroscopy to decompose the overall distribution into contributions from different conformational families.⁴¹ To do so, we first set the CV at fixed values (indicated by colored arrows in Fig. 1(a)), which only admits a

subset of the parent ions into our cold ion trap. We then record UV photofragment spectra of these pre-selected ions, shown in in Fig. 2 for CV values of -7 V, -9 V and -11 V.

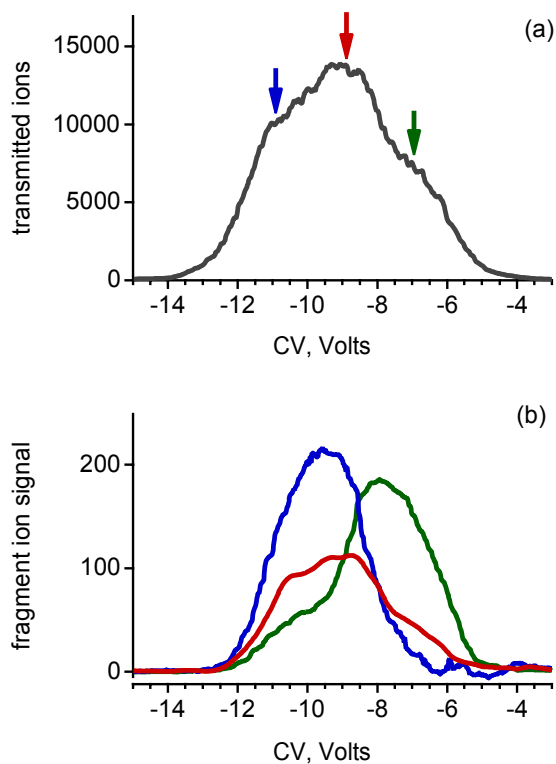


Figure 1. CV spectra of BK^{3+} ; (a) detecting all transmitted ions of BK^{3+} , arrows show the CV values used to record the spectra in Fig. 2; (b) CV spectra recorded *via* UV transitions unique for conformational families I, II and III (arrows in Fig. 2).

The UV spectra taken at the highest and lowest CV values, shown in Figs. 2(a) and (b), have no clear features in common, and these can be attributed to two different conformational families, which we call I and II. The lack of common spectral features indicates that these families are cleanly separated by FAIMS and that no isomerization between them occurs downstream of the separation step. The spectrum of Fig. 2(c), which is taken at $CV=-9V$, contains peaks that belong to families I and II but also unique ones that we assign to a third conformational family (III). To show more clearly the spectral features unique to family III, we subtract the spectra of families I and II with appropriate coefficients from the spectrum of Fig. 2(c). This difference spectrum is displayed in Fig. 2(d).

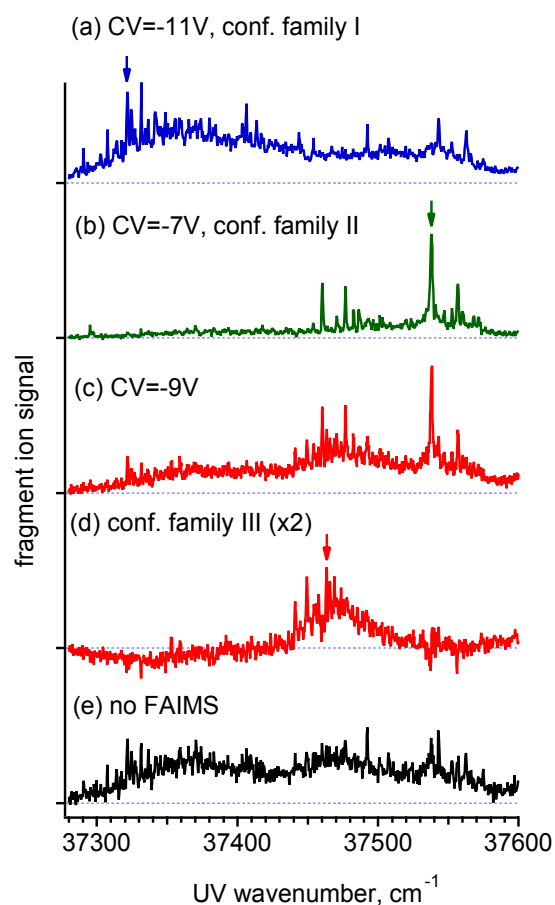


Figure 2. UV photofragmentation spectra of conformational families of BK^{+3} : (a) conformational family I, CV is set to -11V, (b) conformational family II, CV set to -7V, (c) a mixture of conformational families I, II and III, CV set to -9V, (d) conformational family III obtained by subtracting spectra of families I and II from spectrum c, (e) mixture of all conformational families, no FAIMS selection. Arrows show the UV transitions used to record conformer-selective CV spectra in Fig. 1b

With these UV spectra in hand, we can then set the UV laser on a unique spectral feature for each conformational family (37321.6 cm^{-1} for family I, 37538.0 cm^{-1} for family II, and 37463.6 cm^{-1} for family III), shown with arrows in Fig. 2, and scan the CV. This produces a CV distribution for each conformational family, shown in Fig. 1(b). Note that every conformational family may still contain several conformers, which can lead to broadening of each separate CV distribution. Moreover, collisional heating of the molecules during FAIMS separation also contributes to broadening of the peaks and produces shoulders on the CV-distributions of families II and III. Nevertheless, this type of decomposition guides us in pre-selecting different conformational families and in understanding possible interconversion paths between them.

3.2 Spectroscopic evidence for kinetic trapping

The UV photofragment spectrum of the mixture of conformers produced by ESI without the FAIMS separation stage is shown in Fig. 2(e). This mixture should correspond to the same mixture of conformational families observed by Clemmer and coworkers using conventional ion mobility under same solution conditions. In general, we cannot reliably extract the relative abundances of the conformational families from UV photofragment spectra, because the intensities of peaks are determined not only by the number of parent molecules, but also by the absorption cross-section and photofragmentation yield. However, since these parameters remain constant, we can interpret changes in relative intensities of the peaks as changes in number of ions adopting different conformations. We can thus use these spectra to address the question of whether these families are kinetically trapped, high-energy structures or simply represent the most stable gas-phase structures.

To answer this question we compared UV spectra of BK^{+3} with minimal and maximal degrees of collisional activation, using the RF amplitude of our ion funnel to control this. It is possible to change this amplitude from 7V to 90V and still transmit ions into our ion trap, while at higher amplitudes most of the BK^{+3} ions fragment. We thus select one conformational family at a time in FAIMS by fixing the CV on a given value, and then gradually increase the RF amplitude. After collisional activation close to the funnel exit, the ions are thermalized at room temperature in the hexapole pre-trap for 70 ms. The ions are subsequently mass selected and transmitted to the cold ion trap, where they are cooled before the UV photofragment spectrum is recorded.

When conformational family I is selected (Fig. 3(a), CV=-11 V), we initially observe intense absorption bands at 37300-37350 cm^{-1} , which disappear upon increasing collisional activation. At the same time the bands corresponding to families II and III grow in, and at the highest level of activation the distribution of conformers consists exclusively of these two families. This means that conformational family I is kinetically trapped, and its population in the gas-phase after annealing is negligible. When we set the CV at -7 V to select family II and increase the degree of collisional activation (Fig. 3(b)), the spectra indicate that some of the molecules isomerize to conformer family III. The spectrum at high collisional activation is practically identical to the one obtained at CV=-11 V, implying that we reach the same quasi-equilibrium gas-phase distribution independent of the starting conformation. We do not observe the formation of family I, which lies higher in energy than families II and III in the gas phase. Finally, when the CV is fixed at -9 V, the

distribution of conformers at an RF amplitude of 90 V is essentially the same as when families I and III were pre-selected, with no new conformations formed (Fig. 3(c)).

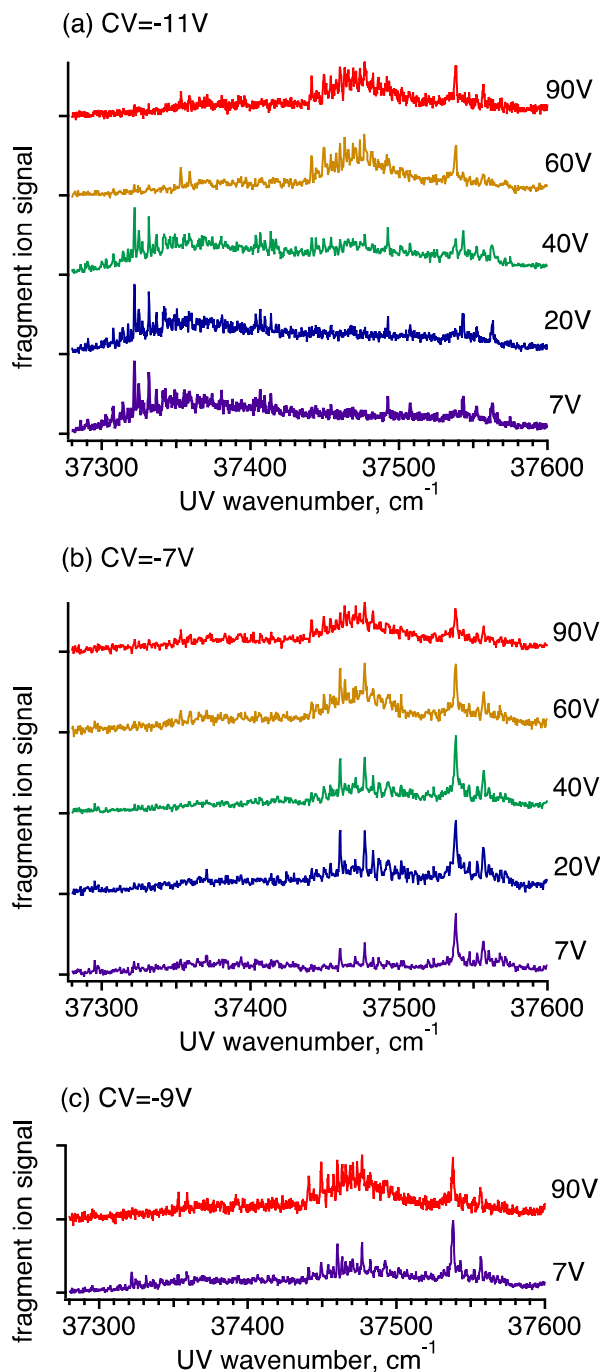


Figure 3. Collisional activation of each conformational family of BK⁺³, preselected by FAIMS. The numbers on the right correspond to the amplitude of the RF voltage on the ion funnel in the source of the spectrometer. (a) Conformational family I converts to a mixture of II and III, (b) conformational family II converts partially to III, (c) the initially selected mixture of families I, II and III converts to the same distribution of stable gas-phase conformers as in a and b

Directly after the ESI process all three conformational families are observed, while after annealing only families II and III are present. Looking only at the distribution of conformations in the gas phase, it is not possible to determine which environment is responsible for stabilizing family I. It may reflect the bulk solution-phase structure, but it could also reflect the specific environment of the electrosprayed droplets. The spectrum of Fig. 3(c) shows that most of the population in conformational family III comes from collisional activation of other families in the gas phase: it is less present than family II even when the CV is set to the maximum of its CV distribution (-9 V), and upon collisional activation its relative intensity increases. However family I is clearly the most important if one is addressing biologically relevant questions about structure and function of the peptide in solution.

The behavior of three peaks separated by FAIMS is similar to that of the three conformational families observed by Clemmer and coworkers using drift-tube IMS.³³ Shvartsburg *et al.* showed previously that there is some degree of correlation between these two separation techniques.⁵⁹ We suggest that what we designate as conformational family I corresponds to what was identified as conformer A in the ion-mobility studies of Clemmer and coworkers.³³ Their drift tube studies show this to be the most compact conformational family, which is confirmed by our spectroscopic studies presented below. The relative abundance of A in their quasi-equilibrium distribution is around 2% of the total number of ions,³³ which is below the signal-to-noise ratio in our experiments, especially taking into account the quite broad UV photofragmentation spectrum of family I.

3.3 Spectroscopic characterization of the conformational families.

The advantage of combining cold-ion spectroscopy with ion mobility is that instead of obtaining a single number, the collisional cross section, with which to characterize a conformation, we can obtain a conformer-specific infrared spectrum, which provides a stringent test of calculated structures. Even without calculations, such spectra can provide qualitative information on structural features. Moreover, we can look in more detail at a conformational family separated by IMS or FAIMS and see how many different individual conformations they contain and identify the structural differences between them. We used double resonance IR-UV spectroscopy to obtain IR spectra of each conformational family in the region of NH and OH stretches. The IR spectra in this region provide information about

the strength of hydrogen bonds, which is enough to distinguish different geometries of the molecule.^{60, 61}

We measure conformer-specific IR spectra by first setting the UV laser on a particular peak in the spectrum and then scanning the frequency of an IR laser pulse that precedes it. When the IR frequency is resonant with a vibrational transition of the conformer that gives rise to the UV transition, it causes a dip or depletion in the UV-induced fragmentation signal. Applying this procedure for all major transitions in the UV photofragment spectrum of conformational family II reveals that there are two distinguishable IR spectra, shown in Fig. 4, and thus two different conformers present, which we call α and β . These two conformers combine to give rise to the UV spectrum of family II.

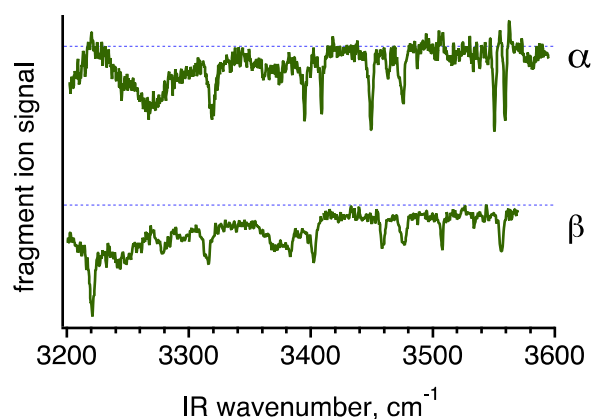


Figure 4. Vibrational spectra of two major conformers of family II: α – UV laser is set on 37460.4 cm^{-1} , β – on 37538 cm^{-1} . The spectra recorded on all the other major transitions in the UV photofragmentation spectra are same as α or β .

We can also use the double-resonance nature of our technique to disentangle the UV spectra of these two conformers. For each conformer we choose a strong band in the IR spectrum that does not appear in the spectrum of other conformer: 3551 cm^{-1} for conformer α and 3556.3 cm^{-1} for the conformer β . The IR laser is then fixed on this wavenumber and the UV laser is scanned. All peaks in the UV photofragmentation spectrum that belong to the IR-labeled conformer will be depleted. By subtracting the UV spectra without and with IR laser we get the UV spectrum of each separate conformer of family II, shown in Fig. 5.

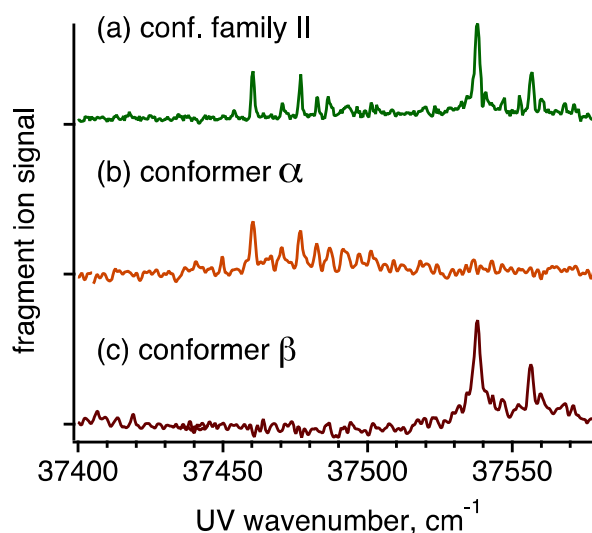


Figure 5. Decomposition of the UV photofragmentation spectrum of family II into a sum of spectra of two conformers, α and β , using IR-UV depletion spectra. Details of the procedure are discussed in the text.

These separate UV photofragment spectra provide some qualitative information about the structure of the conformers giving rise to them. There are two phenylalanine chromophores in BK³⁺, in the fifth and eighth positions in the sequence, and interaction between them could cause exciton splitting of the lines.⁶² We do not observe it for either conformer of family II, suggesting that the side chains of phenylalanines are weakly interacting, either due to a large distance between them or their relative orientation. This provides some guidance for structural searches in future quantum chemical calculations. Moreover, the band origin of conformer β is close to that of bare phenylalanine in the gas phase,⁶³ which means that the chromophores are free from any strong interactions. The band origin of conformer α is significantly red-shifted compared to bare phenylalanine, suggesting a strong cation- π or hydrogen-bonding interaction. Although they belong to the same conformational family, the structures of conformers α and β might be significantly different. The relative intensity of conformer α grows with respect to that of conformer β upon annealing (see Fig. 3(b)), which suggests that the former lies slightly lower in energy. This information could help when searching conformational space to identify the peptide structures of a given conformational family.

The UV photofragmentation spectrum of the kinetically trapped conformational family I is shifted significantly toward lower frequencies, indicating a strong interaction between the chromophores and other parts of the molecule. This is consistent with this structure being the most compact.³³ The IR spectrum of the major conformer of this family, shown in Fig. 6, further supports this statement. The NH stretch bands are red-shifted compared to those of family II, indicating a tighter net of hydrogen bonds. The barrier holding this

metastable structure in place is likely to arise from the competition between this tight hydrogen bonding and the mutual coulomb repulsion between the three charged groups. Upon collisional activation the structure seems to open up, which is confirmed by the larger CCS measured by Clemmer et al.,^{33, 64} the shift of the UV photofragmentation spectrum towards free phenylalanine (Fig. 3(a)), and the blue shift of some of the NH stretch bands.

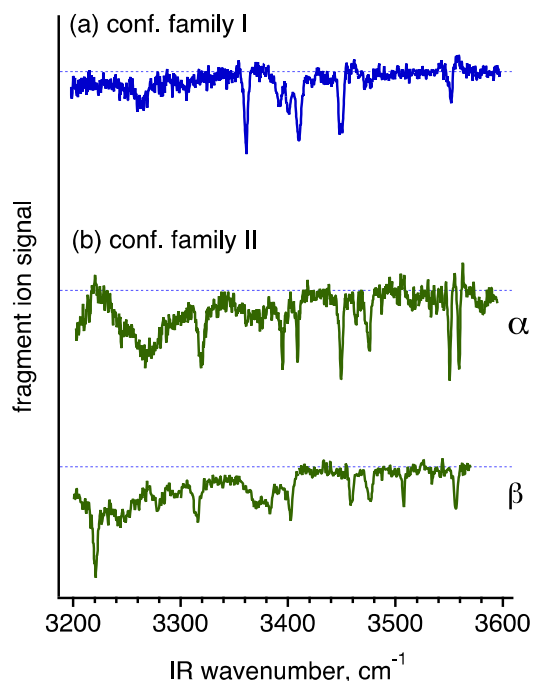


Figure 6. (a) Vibrational spectrum of one of the conformers that belong to kinetically trapped conf. family I, recorded *via* setting UV laser on the strongest transition of family I, 37321.8 cm^{-1} . (b) The spectra of family II are given for comparison.

3.4 Considerations of collisional activation and cooling

To put the conformer distributions that we measure into proper context, it is important to consider the collisional activation and cooling processes that we subject them to. Ions are initially generated by electrospray at room temperature and pressure before being injected into our cold-ion spectrometer. After passing through a metal capillary, they enter the RF ion funnel, where we can activate them (primarily near the exit) by an increase in RF amplitude. After exiting the ion funnel, ions are collisionally cooled in two steps: first during a 70 ms pre-trapping period in a hexapole ion trap at room temperature, and subsequently in the cold ion trap, where the ions collide with cold helium at ~ 4 K. The final distribution of conformers that we observe in the spectroscopic experiments depends not only on the initial distribution of conformations produced by electrospray and the level

of collisional activation in the ion funnel, but also on the rate of cooling. If the ions are cooled significantly faster than the interconversion between different conformers, one obtains a “snapshot” of all the conformations present in the ion cloud before cooling. In this case the spectroscopically observed distribution of conformers reflects the equilibrium distribution corresponding to the initial temperature of the ions. If the cooling process is significantly slower than the isomerization, cooling can be considered as adiabatic process: equilibrium would be established at every given moment, and one would always find one conformer family, as the system would have enough time to interconvert to the lowest-energy conformer. This is obviously not the case in the present experiments, which means that both cooling in the hexapole pre-trap and in the cold octopole trap happen relatively fast. However, the cooling rate in the hexapole should be lower than in IMS experiments due to the lower pressure: 7×10^{-3} mbar compared to several mbar. This can decrease the percentage of higher-energy (i.e., trapped) species in the measured distributions, since they correspond to lower effective temperatures.

3.5 Considerations for benchmarking quantum chemical calculations

The interplay between quantum chemistry calculations and measured vibrational spectra of gas-phase biological molecules is bi-directional. On the one hand, the interpretation of measured spectra requires computed structures and spectra. The normal procedure is to calculate the lowest energy structures and their vibrational spectra, and then compare them to experiment. The experiments are used to select which of the computed structures is the “correct” one, and the calculations are used to interpret the vibrational spectra, particularly in cases where the measured spectra are not assigned. On the other hand, spectroscopic signatures of peptides are frequently used to benchmark quantum chemical calculations.^{60, 61, 65-68} The comparison between calculated and measured IR spectra serve to evaluate the performance of new methods or functionals. For this theory-experiment interplay to work, one needs to know whether measured IR spectra should be associated with the lowest-energy conformations for which the quantum chemical calculations typically search. If the conformations measured in the gas phase do not correspond to the lowest in energy but are kinetically trapped metastable structures, conformational searches may never find them. Moreover, if the accuracy of computational methods is judged by a comparison of the measured spectrum of a metastable species with the calculated spectrum for what is found to be the lowest energy structure, the benchmarking procedure may be completely misguided. From the experimental side, it is

thus important to know when the species one measures may be kinetically trapped, so that computational procedures can be guided to look for higher energy structures. From the computational side, methods need to be implemented to predict how solution phase structures might be trapped during transfer to the gas phase, so that the proper regions of conformational spaces are explored.

Triply protonated bradykinin provides an example of how the interplay between experiment and theory could go wrong. Figure 7 represents the UV photofragmentation spectrum of BK^{+3} , which we originally obtained in our cold-ion spectrometer without any FAIMS pre-selection of conformational families. This spectrum corresponds neither to the stable gas-phase structures exclusively nor to the distribution directly after the electrospray process – it is dominated by conformational family II. Quantum-chemical calculations may thus be misguided by these data. In this case the experimentally observed distribution is practically missing conformational family III, which is formed upon annealing and thus likely to be the lowest-energy in the gas phase. Comparing results of quantum-chemical calculations with the vibrational spectra of family II would explore only a part of all the relevant conformational space of BK^{+3} in the gas phase.

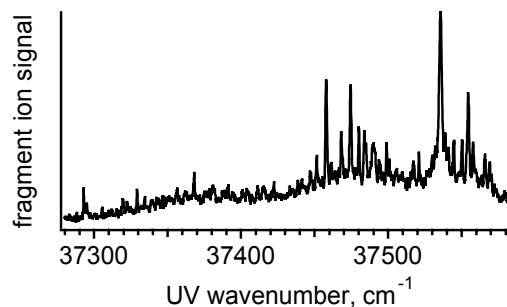


Figure 7. UV photofragmentation spectrum of BK^{+3} , obtained in conditions optimized for maximum of ion signal. No FAIMS separation was applied.

As spectroscopic techniques are pushed to increasingly larger peptides, one would like to measure spectroscopic signatures of kinetically trapped structures, as they may be the most relevant for understanding the function of peptides in solution. Quantum chemical calculations should then be adapted to search for geometry of ions based not only on energy threshold but also on experimental values such as CCS and IR spectra. Modeling of kinetically trapped conformations remains challenging, as they may lie relatively high in energy and are separated from stable gas-phase structures by potential barriers. However, knowledge about their structure is essential to link gas-phase measurements with the structure of biological molecules in solution.

Detailed understanding of the cooling mechanism is also essential for molecular modeling. Relative free energies of different conformers change with temperature,⁶⁶ and measured conformer distributions should be assigned to a particular temperature in order for the comparison between theory and experiment to be correct. If the cooling process in the cold ion trap is assumed to be infinitely fast, the measured distribution reflects distribution of conformers at room temperature.

4 Conclusions

This study provides an overview of an ensemble of conformational families of BK³⁺ in the gas phase. Previously published ion mobility studies allowed separation of conformational families and direct observation of their interconversion.^{33, 64} The double-resonance spectroscopic scheme we employ allows further separation of conformational families into several conformers and facilitates their detailed characterization. We identified three conformational families separated by potential barriers, in agreement with previous ion mobility studies.³³ This confirms that this intrinsically disordered peptide has several well-defined states that are close in energy and can interconvert rapidly. While ion mobility provides a collisional cross section for each conformational family, we have obtained complimentary data such as electronic and vibrational spectra, which can be used as benchmark for quantum chemical calculations of the structures of gas phase BK³⁺. Knowing these structures with atomic precision would allow one to rationalize a vast amount of experimental data obtained for this peptide using different gas-phase techniques and compare them with solution-phase signatures of the conformational ensemble, bringing us closer to understanding the relation between solution-phase and gas-phase structures of biomolecules.

From a biological perspective one is mostly interested in structures that retain some “memory” of solution-phase biologically active states of the peptide. Qualitatively our data confirm that a kinetically trapped structure is compact, in agreement with the expectation that in solution BK also has a relatively compact globular structure as the charges on the side chains are screened by the solvent. However, the biologically active form of BK is extended, has a well-defined S-shape with all Xaa-Pro peptide bonds in the *trans* conformation.⁶⁹ Upon annealing in the gas phase the molecule also expands and might reach a conformation close to that in the presence of biological membranes. However in the gas phase BK³⁺ does not convert to a single structure but to a distribution of conformers, because the cooling rate in our mass spectrometer is fast enough to obtain a

“snapshot” of the distribution of conformers corresponding to some effective temperature. Can this conformational distribution model the biologically active state of BK, as kinetically trapped structures are believed to mimic the state of BK in solution? The spectroscopic signatures of different conformers presented in this study could help us answer this question, expand the use of gas-phase techniques in biological applications and establish limits for their applicability.

5 Acknowledgements

We thank Ecole Polytechnique Fédérale de Lausanne and the Swiss National Science Foundation (through grant 200020_152804) for their generous support of this work.

6 References

1. E. R. Schenk, M. E. Ridgeway, M. A. Park, F. F. Leng and F. Fernandez-Lima, *Anal. Chem.*, 2014, 86, 1210-1214.
2. T. Wyttenbach, N. A. Pierson, D. E. Clemmer and M. T. Bowers, *Annual Review of Physical Chemistry, Vol 65*, 2014, 65, 175-196.
3. D. van der Spoel, E. G. Marklund, D. S. D. Larsson and C. Caleman, *Macromolecular Bioscience*, 2011, 11, 50-59.
4. A. J. R. Heck and R. H. H. van den Heuvel, *Mass Spectrom. Rev.*, 2004, 23, 368-389.
5. C. Uetrecht, R. J. Rose, E. van Duijn, K. Lorenzen and A. J. R. Heck, *Chem. Soc. Rev.*, 2010, 39, 1633-1655.
6. S. Rosati, Y. Yang, A. Barendregt and A. J. R. Heck, *Nature Protocols*, 2014, 9, 967-976.
7. M. Landreh, J. Astorga-Wells, J. Johansson, T. Bergman and H. Jornvall, *Febs Journal*, 2011, 278, 3815-3821.
8. B. C. Bohrer, S. I. Mererbloom, S. L. Koeniger, A. E. Hilderbrand and D. E. Clemmer, *Annual Review of Analytical Chemistry*, 2008, 1, 293-327.
9. D. M. Williams and T. L. Pukala, *Mass Spectrom. Rev.*, 2013, 32, 169-187.
10. R. Beveridge, Q. Chappuis, C. Macphee and P. Barran, *Analyst*, 2013, 138, 32-42.
11. D. Balasubramaniam and E. A. Komives, *Biochimica Et Biophysica Acta-Proteins and Proteomics*, 2013, 1834, 1202-1209.
12. T. Chouard, *Nature*, 2011, 471, 151-153.
13. S. Vahidi, B. B. Stocks and L. Konermann, *Anal. Chem.*, 2013, 85, 10471-10478.
14. L. J. Morrison and V. H. Wysocki, *J. Am. Chem. Soc.*, 2014, 136, 14173-14183.
15. H. Zhang, W. D. Cui and M. L. Gross, *Int. J. Mass Spectrom.*, 2013, 354, 288-291.
16. V. Frankevich, K. Barylyuk, K. Chingin, R. Nieckarz and R. Zenobi, *Chemphyschem*, 2013, 14, 929-935.
17. K. J. Gillig and C.-H. Chen, *Anal. Chem.*, 2013, 85, 2177-2182.
18. G. Papadopoulos, A. Svendsen, O. V. Boyarkin and T. R. Rizzo, *J. Am. Soc. Mass Spectrom.*, 2012, 23, 1173-1181.
19. N. A. Pierson, L. X. Chen, S. J. Valentine, D. H. Russell and D. E. Clemmer, *J. Am. Chem. Soc.*, 2011, 133, 13810-13813.
20. K. Breuker and F. W. McLafferty, *Proc. Natl. Acad. Sci. U. S. A.*, 2008, 105, 18145-18152.
21. B. T. Ruotolo, G. F. Verbeck, L. M. Thomson, K. J. Gillig and D. H. Russell, *J. Am. Chem. Soc.*, 2002, 124, 4214-4215.

22. J. A. Silveira, K. L. Fort, D. Kim, K. A. Servage, N. A. Pierson, D. E. Clemmer and D. H. Russell, *J. Am. Chem. Soc.*, 2013, 135, 19147-19153.
23. R. R. Hudgins, J. Woenckhaus and M. F. Jarrold, *Int. J. Mass Spectrom.*, 1997, 165, 497-507.
24. M. F. Jarrold, *Acc. Chem. Res.*, 1999, 32, 360-367.
25. E. Jurneckzko and P. E. Barran, *Analyst*, 2011, 136, 20-28.
26. T. Wyttenbach and M. T. Bowers, *J. Phys. Chem. B*, 2011, 115, 12266-12275.
27. J. W. Li, J. A. Taraszka, A. E. Counterman and D. E. Clemmer, *Int. J. Mass Spectrom.*, 1999, 187, 37-47.
28. J. A. Loo, J. X. He and W. L. Cody, *J. Am. Chem. Soc.*, 1998, 120, 4542-4543.
29. P. J. Wright, J. M. Zhang and D. J. Douglas, *J. Am. Soc. Mass Spectrom.*, 2008, 19, 1906-1913.
30. H. L. Shi and D. E. Clemmer, *J. Phys. Chem. B*, 2014, 118, 3498-3506.
31. S. Myung, E. R. Badman, Y. J. Lee and D. E. Clemmer, *J. Phys. Chem. A*, 2002, 106, 9976-9982.
32. E. R. Badman, S. Myung and D. E. Clemmer, *J. Am. Soc. Mass Spectrom.*, 2005, 16, 1493-1497.
33. N. A. Pierson, S. J. Valentine and D. E. Clemmer, *J. Chem. Phys. B*, 2010, 114, 7777-7783.
34. J. T. S. Hopper and N. J. Oldham, *J. Am. Soc. Mass Spectrom.*, 2009, 20, 1851-1858.
35. H. Shi, N. Atlasevich, S. Merenbloom and D. Clemmer, *J. Am. Soc. Mass Spectrom.*, 2014, 25, 2000-2008.
36. K. L. Fort, J. A. Silveira, N. A. Pierson, K. A. Servage, D. E. Clemmer and D. H. Russell, *J. Phys. Chem. B*, 2014, 118, 14336-14344.
37. J. A. Silveira, K. A. Servage, C. M. Gamage and D. H. Russell, *J. Phys. Chem. A*, 2013, 117, 953-961.
38. M. Goldstein, L. Zmiri, E. Segev, T. Wyttenbach and R. B. Gerber, *Int. J. Mass Spectrom.*, 2014, 367, 10-15.
39. C. Laphorn, F. Pullen and B. Z. Chowdhry, *Mass Spectrom. Rev.*, 2013, 32, 43-71.
40. S. L. Koeniger, S. I. Merenbloom and D. E. Clemmer, *J. Phys. Chem. B*, 2006, 110, 7017-7021.
41. G. Papadopoulos, A. Svendsen, O. V. Boyarkin and T. R. Rizzo, *Faraday Discuss. Chem. Soc.*, 2011, 150, 243-255.
42. T. R. Rizzo, J. A. Stearns and O. V. Boyarkin, *Int. Rev. Phys. Chem.*, 2009, 28, 481-515.
43. H. Zhu, M. Blom, I. Compagnon, A. M. Rijs, S. Roy, G. von Helden and B. Schmidt, *Phys. Chem. Chem. Phys.*, 2010, 12, 3415-3425.
44. N. S. Nagornova, T. R. Rizzo and O. V. Boyarkin, *Angew. Chem. Int. Ed.*, 2013, 52, 6002-6005.
45. E. M. M. Tan, S. Amirjalayer, S. Smolarek, A. Vdovin, A. M. Rijs and W. J. Buma, *J. Chem. Phys. B*, 2013, 117, 4798-4805.
46. C. Bonechi, S. Ristori, G. Martini, S. Martini and C. Rossi, *Biochimica Et Biophysica Acta-Biomembranes*, 2009, 1788, 708-716.
47. C. Chatterjee and C. Mukhopadhyay, *Biopolymers*, 2005, 78, 197-205.
48. J. K. Young and R. P. Hicks, *Biopolymers*, 1994, 34, 611-623.
49. E. Gaggelli, N. D'Amelio, A. Maccotta and G. Valensin, *European Journal of Biochemistry*, 1999, 262, 268-276.
50. H. Otteleben, M. Haasemann, R. Ramachandran, M. Gorlach, W. MullerEsterl and L. R. Brown, *European Journal of Biochemistry*, 1997, 244, 471-478.
51. R. W. Purves and R. Guevremont, *Anal. Chem.*, 1999, 71, 2346-2357.
52. D. A. Barnett, M. Belford, J.-J. Dunyach and R. W. Purves, *J. Am. Soc. Mass Spectrom.*, 2007, 18, 1653-1663.

53. A. A. Shvartsburg, *Differential Ion Mobility Spectrometry: Nonlinear Ion Transport and Fundamentals of FAIMS*, CRC Press, Taylor and Francis Group,, Boca Raton, FL 33487-2742, USA, 2009.
54. R. Guevremont and R. W. Purves, *Rev. Sci. Instrum.*, 1999, 70, 1370-1383.
55. T. Kim, A. V. Tolmachev, R. Harkewicz, D. C. Prior, G. Anderson, H. R. Udseth, R. D. Smith, T. H. Bailey, S. Rakov and J. H. Futrell, *Anal. Chem.*, 2000, 72, 2247-2255.
56. R. T. Kelly, A. V. Tolmachev, J. S. Page, K. Tang and R. D. Smith, *Mass Spectrom. Rev.*, 2010, 29, 294-312.
57. M. Guidi, U. J. Lorenz, G. Papadopoulos, O. V. Boyarkin and T. R. Rizzo, *J. Phys. Chem. A*, 2009, 113, 797-799.
58. N. A. Pierson, L. X. Chen, D. H. Russell and D. E. Clemmer, *J. Am. Chem. Soc.*, 2013, 135, 3186-3192.
59. A. A. Shvartsburg, F. M. Li, K. Q. Tang and R. D. Smith, *Anal. Chem.*, 2006, 78, 3304-3315.
60. J. A. Stearns, C. Seaiby, O. V. Boyarkin and T. R. Rizzo, *Phys. Chem. Chem. Phys.*, 2009, 11, 125-132.
61. N. S. Nagornova, M. Guglielmi, M. Doemer, I. Tavernelli, U. Rothlisberger, T. R. Rizzo and O. V. Boyarkin, *Angew. Chem. Int. Ed.*, 2011, 50, 5383-5386.
62. N. S. Nagornova, T. R. Rizzo and O. V. Boyarkin, *J. Am. Chem. Soc.*, 2010, 132, 4040-4041.
63. J. A. Stearns, S. Mercier, C. Seaiby, M. Guidi, O. V. Boyarkin and T. R. Rizzo, *J. Am. Chem. Soc.*, 2007, 129, 11814-11820.
64. N. A. Pierson and D. E. Clemmer, *Int. J. Mass Spectrom.*, DOI: <http://dx.doi.org/10.1016/j.ijms.2014.07.012>.
65. M. Doemer, M. Guglielmi, P. Athri, N. S. Nagornova, T. R. Rizzo, O. V. Boyarkin, I. Tavernelli and U. Rothlisberger, *International Journal of Quantum Chemistry*, 2013, 113, 808-814.
66. M. Rossi, V. Blum, P. Kupser, G. von Helden, F. Bierau, K. Pagel, G. Meijer and M. Scheffler, *J. Phys. Chem. Lett.*, 2010, 1, 3465-3470.
67. C. Baldauf, K. Pagel, S. Warnke, G. von Helden, B. Koksche, V. Blum and M. Scheffler, *Chem.-Eur. J.*, 2013, 19, 11224-11234.
68. S. Jaesqx, J. Oomens, A. Cimas, M. P. Gageot and A. M. Rijs, *Angew. Chem. Int. Ed.*, 2014, 53, 3663-3666.
69. J. J. Lopez, A. K. Shukla, C. Reinhart, H. Schwalbe, H. Michel and C. Glaubitz, *Angew. Chem. Int. Ed.*, 2008, 47, 1668-1671.